Sun *et al.*
Chinese Journal of Mechanical Engineering (2022) 35:129
https://doi.org/10.1186/s10033-022-00804-2

Chinese Journal of Mechanical Engineering

ORIGINAL ARTICLE Open Access

Laser Oscillating of Nickel Alloyed Welds on Press-Hardened Steel

Qian Sun[1], Zhenghui Zhang[2], Xiaonan Wang[2*], Qingyu Zhang[2*] and Zhenguang Liu[3]

Abstract

Laser oscillating welding was employed to fabricate Al-Si coated press-hardened steel (PHS) to improve the element homogeneity in the fusion zone. Laser oscillating welding was employed with various oscillation amplitudes (0 mm, 0.5 mm and 1.3 mm) in this present. Ni foil of 0.06 mm thickness was used as an interlayer between two tailored PHS welded. The weld morphology, elemental profile, microstructure and tensile strength of welded joints were studied. The results showed that full penetration weld without any weld defects were achieved for any oscillation amplitudes, and weld width increased with increasing oscillation amplitudes. With the oscillation amplitudes increased, Ni and Al had an uneven elemental profile due to strong stirring force, but the Ni and Al content in the weld was decreased and Ni had a sharp descent compared to Al element. Only few δ-ferrite was presented in fusion line with the oscillation amplitudes increased to 1.3 mm. The oscillation amplitudes did not have an effect on the tensile properties, which was similar to that of base metal. But if keeping increasing the oscillation amplitudes or reducing the thickness of Ni interlayer, it has a potential risk to form more and more δ ferrite such that deteriorate the mechnical properties of welded joints.

Keywords: Laser oscillating welding, Al-Si coating, Press-hardened steel, Nickel alloyed, Microstructure and properties

1 Introduction

Press hardened steel (PHS), commonly used in automotive anti-collision beam, front and rear bumpers, A column, B column and the middle passage and other important compounds due to its ultra-high tensile strength after hot stamping process [1–4]. Generally, Al-Si coating is employed on the surface of steel to avoid excessive oxidation during hot stamping [5]. Laser welding is a subject of interest on the joining of Al-Si coated PHS, due to the advantages of narrow heat affected zone, low heat input and high welding speed, etc [6, 7]. Unfortunately, the Al-Si coating is also melted during laser welding and diffuses into molten pool to deteriorate the properties of welded joints. Studies showed that the formation of δ-ferrite with high Al content has the responsibility for this, since Al was a stabilizer of austenite [8–10].

The presence of δ-ferrite phase limits the application of PHS during the actual manufactures, many studies on the suppression of the formation of δ-ferrite phase were carried out [11–17]. Lin et al. [13] introduced a carbon-steel filler to dilute the Al segregation. The results showed that narrow and small strips were formed instead of original large and long δ-ferrite, which boost the Al dilution in the fusion zone and improved the joint strength. Kang et al. [14] found that larger laser beam can improve the homogenization of Al to inhibit the segregation in the fusion zone and increased the fraction of martensite. In our previous studies, we found that partial primary δ-ferrite at high temperature did not go through phase transformation and then remained to room temperature, which was the key for the reduction of joint strength [15]. In addition, Ni foil was used as an interlayer between the

*Correspondence: wxn@suda.edu.cn; qingyu.zhang@suda.edu.cn

[2] Shagang School of Iron and Steel, Soochow University, Suzhou 215137, China
Full list of author information is available at the end of the article

Table 1 Chemical composition of test steel (wt.%)

C	Si	Mn	Ti	Cr	Al	B	N	P	S	Fe
0.23	0.27	1.13	0.04	0.16	0.037	0.0025	0.004	0.012	0.001	Balance

two tailor welded sheets during laser welding [16, 17]. Ni reduced the fraction of primary δ-ferrite, but excessive Ni content could result in the formation of austenite in the fusion zone.

Generally, the gap tolerance and weld quality is also an important issue for laser welding. Thus, the laser welding with beam oscillating was founded, called laser oscillating welding [18], which can improve the gap tolerance and reduce the weld defects, especially in the dissimilar laser welding [19, 20]. Laser heat source could be oscillated periodically through scanning mirrors, either sinusoidal, circular or other complex oscillation tracks [21]. Recently, laser oscillating welding has been paid more and more attention, not only reducing the weld defects, but also improving the stirring efficiency of molten pool and grain refinement to prevent the generation of macrosegregation [22, 23]. Zhao et al. [24] studied the effect of laser oscillating beam on the porosity of low carbon steel. The results showed that the oscillating can reduce and eliminate the porosity during laser welding, and increased oscillating frequency and diameter was beneficial for the escape of bubbles from the molten pool. Jiang et al. [23] suggested that oscillating laser source could achieve grain refinement and decrease internal defects during laser welding of Invar alloy. Furthermore, a homogeneous elemental profile was achieved in the dissimilar laser oscillating welding of Ni–Cr–Mo and Cu–Cr–Zr alloys [22]. Gerhards et al. [25] tried the investigation of Al-Si coated 22MnB5 PHS with laser oscillating welding, the results showed that Al segregation along the fusion line was diluted, the joint strength was improved but still less than base metal.

In our previous studies, the insert of Ni foil as an interlayer can suppress the formation of δ-ferrite in the fusion zone, but non-fusion was also present during laser welding. More to the point, it was difficult to achieve the precise control of Ni foil thickness. Thus, laser oscillating was introduced to weld Al-Si coated PHS with Ni interlayer, and various oscillation amplitudes was carried out in this present. This work is an effort to fill the gap in the literature and investigate of Al-Si coated tailored laser welding and create possible potential technology.

2 Experimental Procedure

In this study, 22MnB5 press-hardened steel (PHS) with Al-Si coating on double sides were used, 1.5 mm thickness. The chemical composition is listed in Table 1.

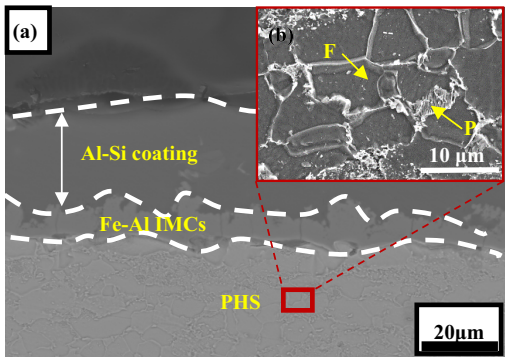

Figure 1 The microstructure characterization of Al-coating on PHS: **a** Coating distribution, **b** microstructure

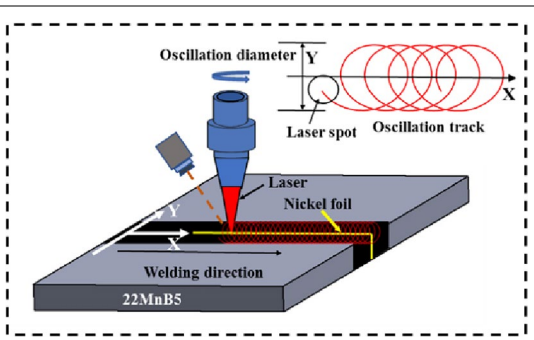

Figure 2 Schematic sketches of laser oscillation welding

Al-Si coating, Fe-Al IMCs was observed from outer to inner on the PHS surface (Figure 1a), and the microstructure consisted of ferrite (F) and pearlite (P) (Figure 1b).

The laser welding was employed by IPG YLS-6000 fiber laser with mechanical swing, which can achieve two welding modes. The oscillation amplitudes were set as 0 mm to achieve conventional laser linear welding, and oscillation amplitudes was set as 0.5 and 1.3 mm to achieve laser oscillating welding. The laser beam track path during laser oscillation welding was selected as shown as in Figure 2. Ni foil of 0.6 mm thickness was prepared between two tailored welded sheets as an interlayer. The parameters of laser oscillating welding is listed in Table 2.

The in-situ observation of molten pool morphologies was carried out by using high-speed camera. Samples

Table 2 The parameters of laser oscillating welding

Oscillation amplitudes A_{osc} (mm)	Laser power (kW)	Welding speed (m/min)	Oscillation speed (mm/s)	Nickel foil thickness (mm)
0	2.3	5	0	0.06
0.5	2.3	5	800	0.06
1.3	2.3	5	800	0.06

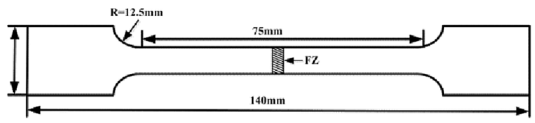

Figure 3 Sample drawings of tensile test

were polished and etched with 4% natal, and then the microstructure and fracture images were captured by Zeiss optical microscopy (OM), SU5000 scanning electron microscope (SEM), and transmission electron microscope (TEM). The elemental distribution was analyzed by Oxford x-max20 energy dispersive spectroscopy (EDS). HV-1000 microhardness tester was used to measure the microhardness, tensile test was implemented on DNS-100 universal testing machine (Figure 3).

3 Results and Analysis

3.1 Weld Appearance

Figure 4 presents the weld surface aspect and cross-section profiles with different oscillation amplitudes. Smooth weld and full penetration was achieved for all the samples, with the absence of weld defect (Figure 4a–c). It was clear that increasing the oscillation amplitude, the weld size was significantly expanded at the top and bottom surface, and the weld width increased from ~ 384 μm (A_{osc}=0) to 1248 μm (A_{osc}=1.3), and the weld shape was altered from hourglass to an inverted trapezoid shape. Compared to Figure 4d and e, the weld width only had a slightly increase with the addition of oscillation for stirring (A_{osc}=0→A_{osc}=0.5), but it was evident with oscillation amplitude increased to 1.3 mm (Figure 4f).

Previous studies showed that heat input had a significant effect on the weld width, depending on the weld speed, peak power, etc. In this study, the welding parameters were constant, but with various laser oscillation amplitudes. Compared to linear laser beam, the oscillating laser beam is in fact a spiral one since the beam is continuously moving in the weld direction. Figure 5 presents the schema of the laser beam oscillation during a circular movement. For linear laser welding, the melting metal area was depended on the single laser beam, and its welding speed was equal to the moving speed of the steel plate. However, when

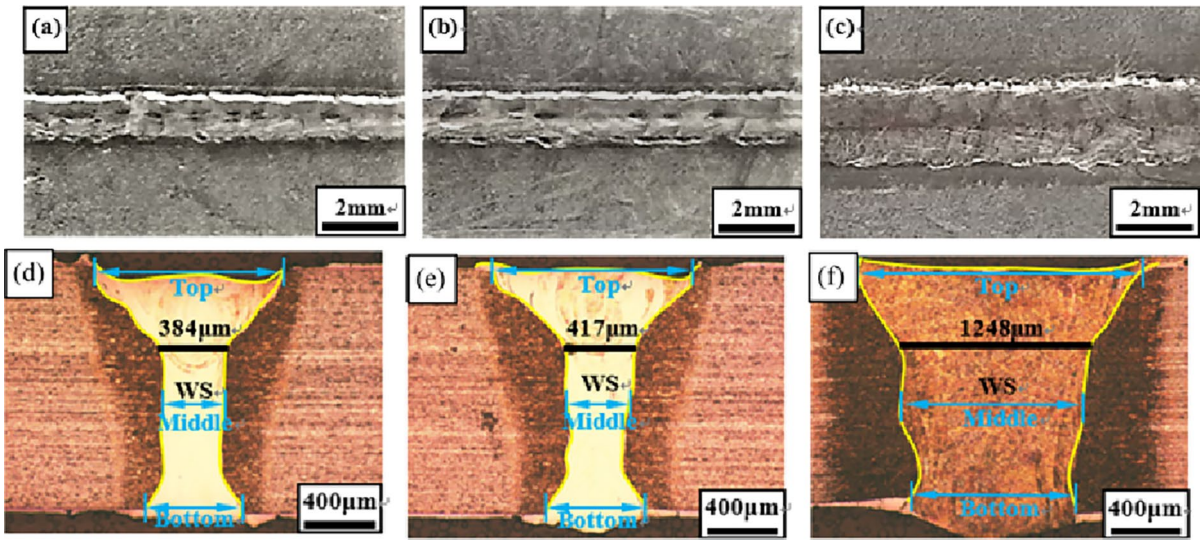

Figure 4 Weld profile with different oscillation amplitudes: **a** Top surface for without oscillating($A_{osc=0}$), **b** top surface for $A_{osc=0.5}$, **c** top surface for $A_{osc=1.3}$, **d** cross section for without oscillating($A_{osc=0}$), **e** cross section for $A_{osc=0.5}$, **f** cross section for $A_{osc=1.3}$

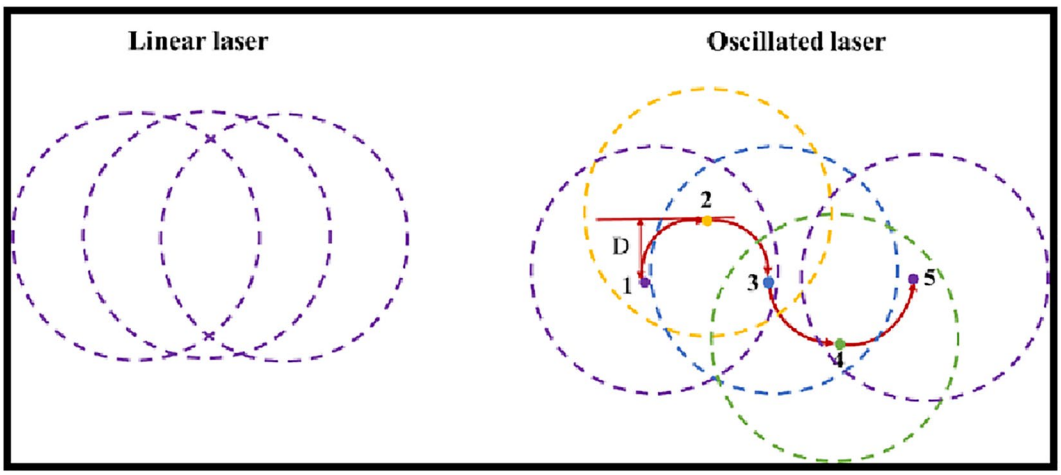

Figure 5 Schema of the laser beam oscillation during a circular movement

applied oscillation, interaction area on the welded metal was increased, which was determined by the oscillation amplitudes. The greater oscillation amplitudes, the larger interaction area is. As a result, a wider molten pool can be formed due to more melting welded metals. Thus, the top weld size had a corresponding results after welding cooling and solidification. While, the oscillation amplitudes was 0.5 mm, the weld width had a slightly increase compared to the case of without oscillating ($A_{osc} = 0$). Laser energy distribution on weld appearance maybe the key, as shown in Figure 6, similar results were also presented in Ref. [23]. When $A_{osc} = 0.5$, the peak energy in the center had a slightly reduce compared to Aosc = 0, as well as no evident increase for energy interaction areas. Thus, the weld width was similar for $A_{osc} = 0$ (0.38 mm) and A_{osc}=0.5 (0.4 mm), but it was increased to 1.6 mm with oscillation amplitudes was 1.5 mm. Compared to Ref. [23], full penetration weld was achieved with different oscillation amplitudes, since the weld depth and width was also determined by other welding parameters, such as welding speed, oscillation frequency, and so on.

3.2 Elements in the Fusion Zone

Ni foil was applied as interlayer during Al-Si coated PHS laser welding in this study. This present focused on the distribution of Ni and Al with different oscillation amplitudes, as shown as in Figure 7. As mentioned in Sect. 3.1, the weld width was increasing with oscillation amplitudes increased. Actually, the weld width was also different from top surface to bottom surface, especially in a transition zone where the size had a sharp cut-down, located in the neck of fusion zone (Marked by red rectangle in Figure 4). For linear laser ($A_{osc} = 0$), the content of Ni and Al had a great variation in the fusion zone, and segregation was evident in the transition zone (Figure 7a and d). With the oscillation amplitudes increased to 0.5 mm, although the weld shape was similar to linear laser,

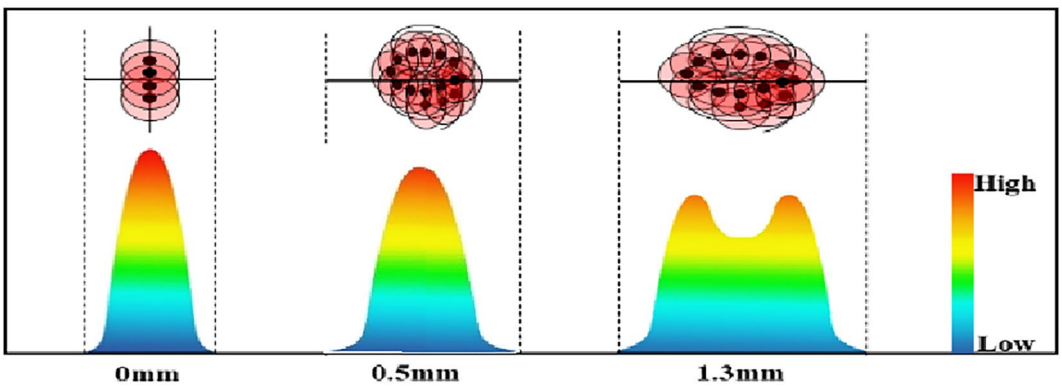

Figure 6 Schematic illustration of energy distribution [23]

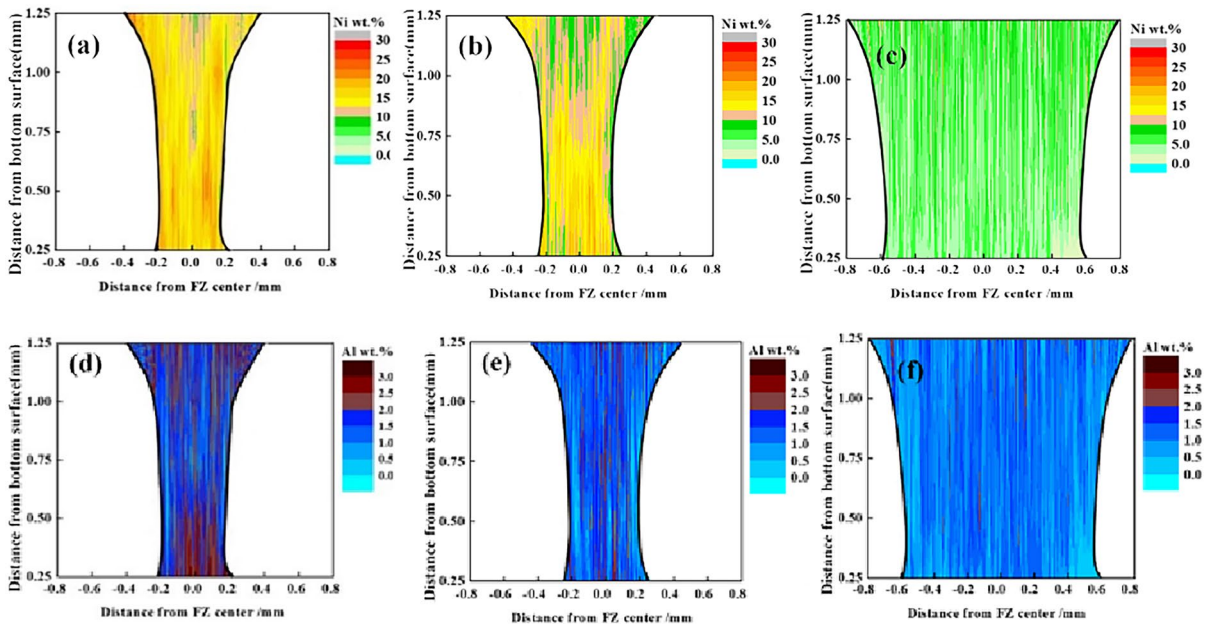

Figure 7 Elemental distribution in fusion zone with different oscillation amplitudes: **a** $A_{osc=0}$, Ni, **b** $A_{osc=0.5}$, Ni, **c** $A_{osc=1.3}$, Ni, **d** $A_{osc=0}$, Al, **e** $A_{osc=0.5}$, Al, **f** $A_{osc=1.3}$, Al

but the segregation was not visible in the transition zone (Figure 7b and e). When the oscillation amplitudes was 1.3 mm, Al had a more uneven distribution than A_{osc}=0 and A_{osc}=0.5 (Figure 7f). Furthermore, a homogeneous content profile for Ni was achieved in the fusion zone, as shown as in Figure 7c.

Generally, the melt flow in the molten pool has a significant influence on the elemental distribution in the fusion zone. Based on the previous studies [26–28], this present established a module to understand the elemental flow in the molten pool during laser welding, as shown as in Figure 8. Al–Si layer coated on the both surfaces of PHS was melted under the effect of laser radiation, and then diffused into the molten pool. Ni interlayer, was also melted with the base metals during laser welding. In this module, we regarded Ni and Al as spherical Ni-rich and Al-rich particles in the molten pool. Here, two melt flow loops were formed by the effect of Marangoni force and keyhole, respectively. It was upper flow loop in the upper half of the molten pool, and lower flow loop in the down half [26]. Ni-rich and Al-rich particles were flowing with melt metals. However, the presence of the transition zone was considered as the block for these particles flow due to the cup-shaped, resulted in an elemental stacking in

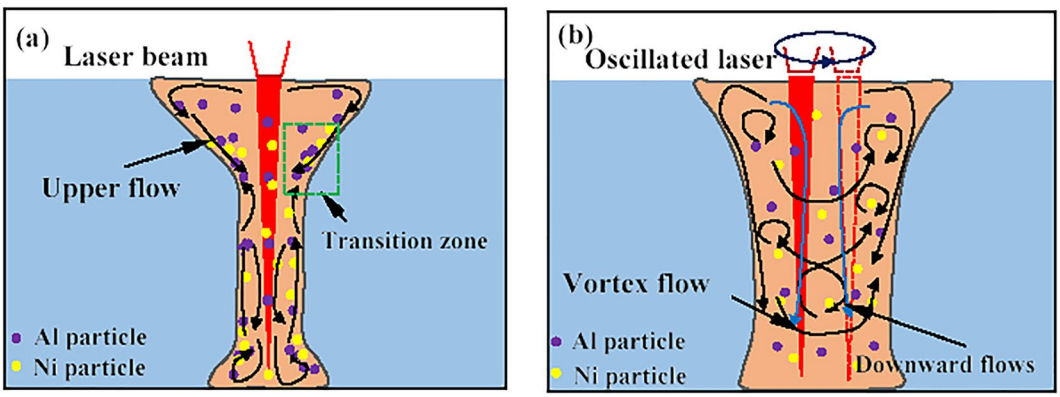

Figure 8 Schematic illustration of the elemental flow: **a** $A_{osc=0}$, **b** $A_{osc=1.3}$

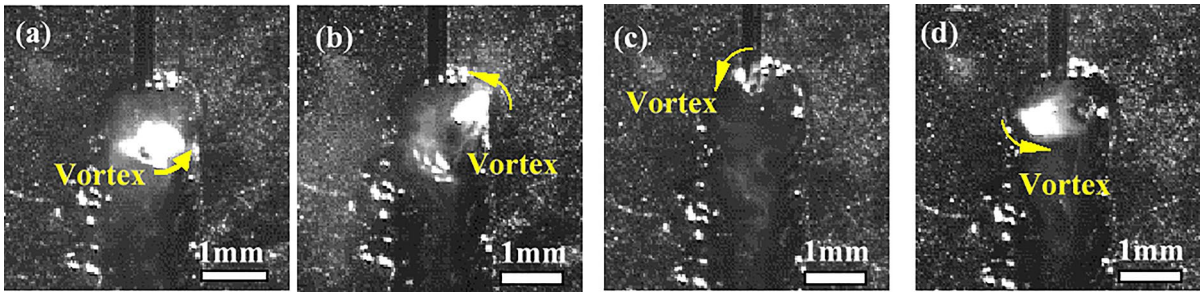

Figure 9 Laser beam path in a rotary moving cycle

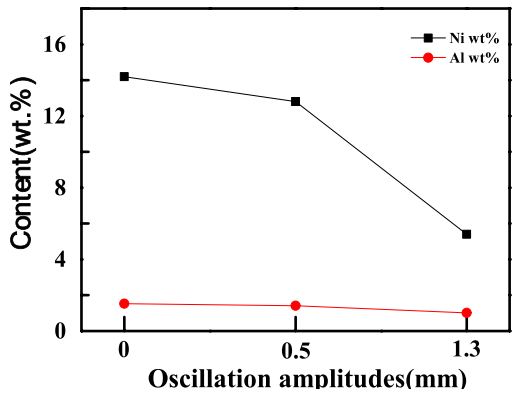

Figure 10 Average elemental contents in the fusion zone with different oscillation amplitudes

this zone (Figure 8a). Thus, it was clear that Ni and Al had a visible segregation in the transition zone with high content for the linear laser. With the oscillation applied, the laser beam has a rotary moving to provide a stirring force in the molten pool (Figure 9). Hence, the stacking particles were driven to migrate to the whole molten pool (Figure 8b), the greater oscillation amplitudes, and the more evident stirring effect. It provided an evidence for elemental distribution difference when the oscillation amplitudes increased from 0 to 1.3 mm. Although similar weld size and shape was for $A_{soc} = 0$ and $A_{soc} = 0.5$, but the presence of oscillation weakened the segregation in the transition zone (Figure 8b), and a homogeneous element profile for $A_{soc} = 1.3$ was achieved as a result.

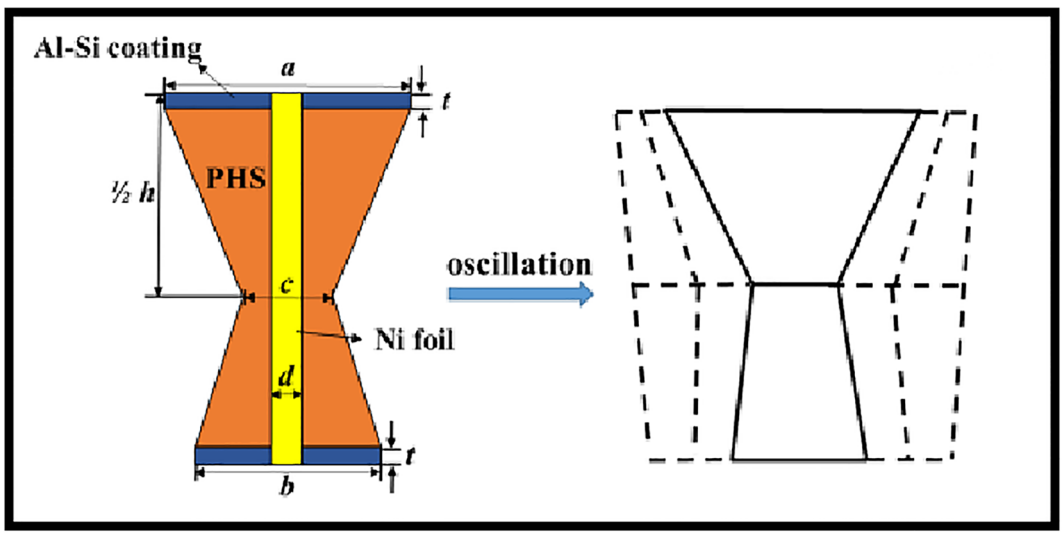

Figure 11 Simplified weld shape with increasing oscillation amplitudes

In addition, it was further found that the average content of Al and Ni was decreased with increasing oscillation amplitudes, as shown as in Figure 10. In order to calculate the average elemental content in the fusion zone, this present regarded the weld as a simplified shape, as shown as in Figure 11. Where, a is the width of top surface, mm; b is the width of bottom surface, mm; c is the width of half part, mm; t is the thickness of Al-Si coating, mm; h is the thickness of PHS plate,1.5 mm; d is the thickness of Ni foil, 0.06 mm; S is the area of weld cross-section. Based on this, the Ni content can be calculated as Eq. (1). It was clear that ω_{Ni} was determined by the area of cross-section of fusion zone, S, which depended on the oscillation amplitudes (d is a constant value, 0.06 mm). Thus, the average Ni content in the fusion zone decreased with oscillation amplitudes increased.

$$\omega_{\mathrm{Ni}} = \frac{dh \cdot \rho_{\mathrm{Ni}}}{S\rho_{\mathrm{Fe}}}, \tag{1}$$

$$\begin{aligned}\omega_{\mathrm{Al}} &= \frac{(a+b)t\rho_{\text{Al-Si}} \cdot 0.9}{S\rho_{\mathrm{Fe}}} = \frac{(a+b)t\rho_{\text{Al-Si}} \cdot 0.9}{\left(\frac{a+c}{2} \cdot \frac{1}{2}h + \frac{b+c}{2} \cdot \frac{1}{2}h\right) \cdot \rho_{\mathrm{Fe}}} \\ &= A \cdot \frac{a+b}{a+b+2c} = A \cdot \frac{1}{1+\frac{2c}{a+b}}, A = \frac{3.6t\rho_{\text{Al-Si}}}{h\rho_{\mathrm{Fe}}}.\end{aligned} \tag{2}$$

By this means, the Al content was calculated as Eq. (2), it equals the weight of Al divided by the weight of fusion zone. Combined with Figure 11, the weld shape was altered from hourglass to an inverted trapezoid shape, $\frac{2c}{a+b}$, which was increasing with oscillation amplitudes increased, such that a decreasing Al content. When the weld altered to inverted trapezoid shape, $c \approx \frac{a+b}{2}$, it means that the average Al content in the fusion zone will be a constant nerveless of any oscillation amplitudes. In contrast, the average Ni content will be decreased sharply due to the constant thickness of Ni foil. Thus, it was considered that the descent of average Al content had a slow trend compared to Ni content.

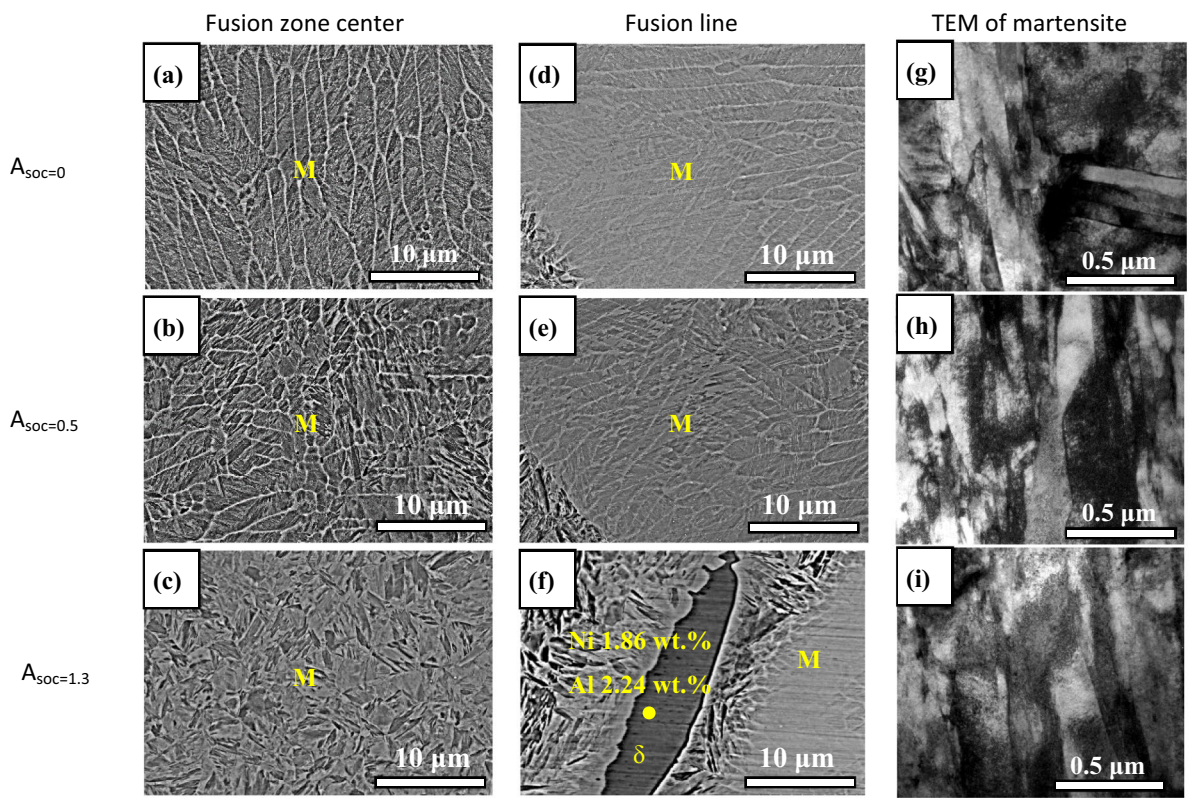

Figure 12 Microstructure in fusion zone and fusion line with different oscillation amplitudes

3.3 Microstructure and Properties

Figure 12 presents the microstructure in the fusion zone (FZ) center and fusion line (FL). Similar microstructure was observed in the FZ center and FL for the case of $A_{osc} = 0$ and $A_{osc} = 0.5$ (Figure 12a, b, d and e). Martensite was confirmed by TEM results (Figure 12g and h). With the oscillation amplitudes increased to 1.3 mm, a different microsturcture profile was achieved in the FZ center, maybe it was another phase. While, TEM image (Figure 12i) cleared away this uncertainty, the visible lath martensite was found in the weld center. In addition, δ-ferrite was present in the fusion line [8–10].

In our previous studies [15–17], the formation of δ-ferrite was determined by the Al content in the molten pool since Al was an austenite stabilizer, while the presence of Ni can promote the formation of austenite. In this present, although the Ni interlayer has a constant thickness, but the oscillation amplitudes was altered from 0 to 1.3 mm, such that a decreased Ni content in the fusion zone, as mentioned as in Sect. 3.2. JMatPro was used to calculate the phase fraction of fusion zone, based on the average elemental contents, as shown as in Figure 13. As can be seen in Figure 13a–c, the liquid phase completely transformed into austenite without any presence of high-temperature ferrite, and followed by transforming into martensite via shear phase transformation during solidification. Compared to $A_{soc} = 0$ and $A_{soc} = 0.5$, martensite phase had a different microstructure profile, which was occupied by different Ni content. However, δ-ferrite was persent along the FL with the oscillation amplitudes increased to 1.3 mm, the phase transformation was presented in Figure 13d. It was showed that 8% of high temperature ferrite did not transform into austenite, and remained to the room temperature to form δ-ferrite. In this case, the Ni content was not sufficent to suppress the formation of δ-ferrite, since the Ni content in the fusion zone had a sharp descent compared to Al.

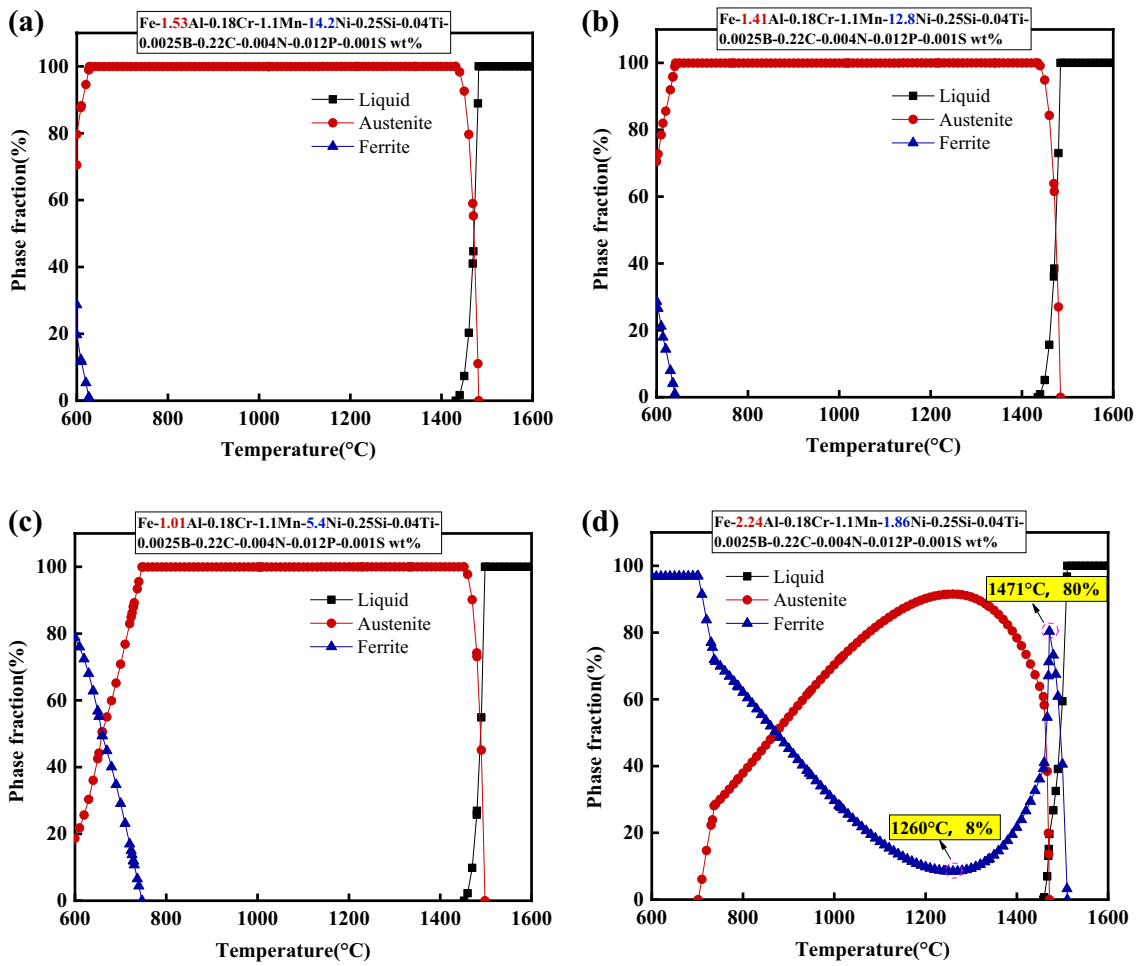

Figure 13 Simulated phase transformation by JMatPro with different oscillation amplitude: **a** $A_{soc=0}$ in FZ, **b** $A_{soc=0.5}$ in FZ, **c** $A_{soc=1.3}$ in FZ, **d** $A_{soc=1.3}$ in FL

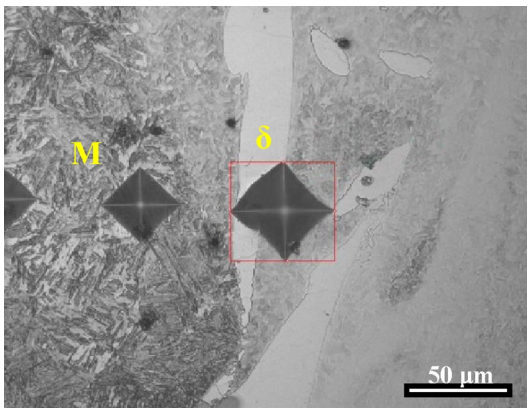

Figure 14 Local hardness indentation near to fusion line of $A_{osc=1.3}$

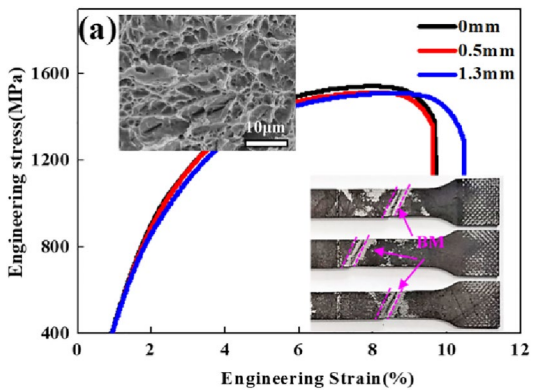

Figure 15 Tensile results of heat-treatment welded joints with different oscillation amplitude

Hence, the microstructure of fusion zone was lath martensite with the oscillation amplitudes increased from 0 to 1.3 mm, but the increasing oscillation amplitudes also provided a potential for the formation of δ ferrite due to the sharp descent of Ni content in the fusion zone.

Actually, the laser tailored sheet of PHS is followed by hot-stamping. Thus, heat treatment was used in this present to get the welded joints similar to the actual manufacture. The fusion zone had similar average hardness (~ 498HV) for any oscillation amplitudes, due to the martensite microstructure. However, a very narrow area with low hardness (~ 299HV) was found near to the fusion line for $A_{soc} = 1.3$, as shown as in Figure 14. As mentioned, δ-ferrite formed in the fusion line in Figure 12f, and it did not go through phase transformation during heat treatment, only with the grain boundary migration. Thus, the presence of softer ferrtie had the reasonability for the hardness reduction due to lower hardness than martensite.

Figure 15 presents the tensile properties for the welded joints. The results showed that the increasing oscillation amplitudes in this present did not have an influence on the tensile strength and elongation of welded joints, and fracture failed in the base metal (BM). Dimples were in the fracture surface, implying as ductile fracture. Previous studies [16, 28, 29] had been confirmed that the presence of δ-ferrite was the key for the strength decrease of welded joint. In this present, the fracture location of $A_{soc=1.3}$ was in base metal although little δ-ferrite was in fusion line, maybe due to the strain constraint from surrounding hard phase. Anyway, the presence of δ-ferrite in the fusion zone was not recommended in the actual manufacture.

4 Conclusions

Laser oscillating welding was employed with various oscillation amplitudes aimed at Al-Si coated PHS with Ni interlayer in this present. The main conclusions was drawn as the following:

(1) With the oscillation amplitudes increased, the laser interaction area on the welded metals were enlarged, resulted in a greater weld size. The weld defects were absent for any condition of oscillation amplitudes, and full penetration was achieved.
(2) Under the effect of oscillation amplitudes, Ni and Al contents in the fusion zone tended to be homogeneous. The contents of both elements in the fusion zone decreased with oscillation amplitudes increased, but Ni had a sharp descent compared to Al. The microstructure was lath martensite with the oscillation amplitudes increased to 0.5 mm, and few δ-ferrite was present for the condition of 1.0 mm oscillation amplitudes.
(3) With the oscillation amplitudes increased, the tensile strength of welded joints was still similar to the base metal, although the presence of few δ-ferrite when the oscillation amplitudes was 1.0 mm. The study indicates that increasing the oscillation amplitudes or reducing the thickness of Ni interlayer has a potential risk to form more δ ferrite such that deteriorate the mechnical properties of welded joints.

Acknowledgements
Not applicable.

Authors' Contributions
XW and QZ as in charge of the whole trial; QS wrote the manuscript; ZZ and ZL assisted with sampling and laboratory analyses. All authors read and approved the final manuscript.

Authors' information
Qian Sun, born in 1985, is a PhD at *School of Mechanical and Electrical Engineering, Soochow University, Suzhou, China*. She received her PhD degree from *Northeastern University, China*, in 2020. Her research interests include laser welding of high strength steels. E-mail: qiansun@suda.edu.cn.
Xiaonan Wang, born in 1984, is a professor at *Shagang School of Iron and Steel, Soochow University, Suzhou, China*. E-mail:wxn@suda.edu.cn.
Qingyu Zhang, born in 1988, is an associate professor at *Shagang School of Iron and Steel, Soochow University, Suzhou, China*. E-mail: qingyu.zhang@suda.edu.cn.
Zhenghui Zhang, born in 1996, a master candidate at *Shagang School of Iron and Steel, Soochow University, Suzhou, China.*
Zhenguang Liu, is an associate professor at *Jiangsu University of Science and Technology, Zhenjiang, China.*

Funding
Supported by National Natural Science Foundation of China (Grant No. 52005357), "Qinglan" Project of Jiangsu Province of China, and Jiangsu Provincial Natural Science Foundation of China (Grant No. BK 20180984).

Competing interests
The authors declare no competing financial interests.

Author Details
[1]School of Mechanical and Electrical Engineering, Soochow University, Suzhou 215137, China. [2]Shagang School of Iron and Steel, Soochow University, Suzhou 215137, China. [3]School of Materials Science and Engineering, Jiangsu University of Science and Technology, Zhenjiang 212000, China.

Received: 28 August 2021 Revised: 28 September 2022 Accepted: 29 September 2022
Published online: 22 October 2022

References

[1] P Hein, J Wilsius. Status and innovation trends in hot stamping of usibor 1500P. *Steel Research International*, 2008, 79(2):85-91.
[2] J Wang, C Enloe, J Singh, et al. Effect of prior austenite grain size on impact toughness of press hardened steel. *SAE International Journal of Materials and Manufacturing*, 2016, 9(2):488–493.
[3] K R Jo, L Cho, D Sulistiyo, et al. Effects of Al-Si coating and Zn coating on the hydrogen uptake and embrittlement of ultra-high strength press-hardened steel. *Surface & Coating and Technology*, 2019, 374: 1108–1119.
[4] L Golem, L Cho, J Speer, et al. Influence of austenitizing parameters on microstructure and mechanical properties of Al-Si coated press hardened steel. *Materials & Design*, 2019, 17:107707.
[5] H Karbasian, A E Tekkaya. A review on hot stamping. *Journal of Materials Processing Technology*, 2010, 210(2): 2103-2118.
[6] L Zhang, L Bai, J Ning, et al. A comparative study on the microstructure and properties of copper joint between MIG welding and laser-MIG hybrid welding. *Materials & Design*, 2016, 110:35-50.
[7] J Xue, P Peng, W Guo, et al. HAZ characterization and mechanical properties of QP980-DP980 laser welded joints. *Chinese Journal of Mechanical Engineering*, 2021, 34: 80.
[8] X Gao, L Zhang, J Liu, et al. Porosity and microstructure in pulsed Nd: YAG laser welded Ti6Al4V sheet. *Journal of Materials Processing Technology*, 2014, 214(7): 1316-1325.
[9] D C Saha, E Biro, A P Gerlich, et al. Fusion zone microstructure evolution of fiber laser welded press-hardened steels. *Scripta Materialia*, 2016, 121:18–22.
[10] D C Saha, E Biro, A P Gerlich, et al. Fiber laser welding of Al-Si coated press hardened steel. *Welding Journal*, 2016, 95:147–156.
[11] M Shehryar, M H Razmpoosh, E Biro, et al. A review on the laser welding of coated 22MnB5 press-hardened steel and its impact on the production of tailor-welded blanks. *Science and Technology of Welding and Joining*, 2020, 25: 447–467.
[12] M Shehryar, S I Shahabad, M Yavuz, et al. Numerical modelling and experimental validation of the effect of laser beam defocusing on process optimization during fiber laser welding of automotive press-hardened steels. *Journal of Manufacturing Processes*, 2021, 67: 535–544.
[13] W Lin, F Li, X Hua, et al. Effect of filler wire on laser welded blanks of Al-Si-coated22MnB5 steel. *Journal of Materials Processing Technology*, 2018, 259: 195–205.
[14] M Kang, Y M Kim, C Kim. Effect of heating parameters on laser welded tailored blanks of hot press forming steel. *Journal of Materials Processing Technology*, 2016, 228: 137–144.
[15] X Wang, X Chen, Q Sun, et al. Formation mechanism of δ-ferrite and metallurgy reaction in molten pool during press-hardened steel laser welding. *Materials Letters*, 2017, 206C:143-145.
[16] Q Sun, H Di, X Wang, et al. Suppression of δ-ferrite formation on Al-Si coated press hardened steel during laser welding. *Materials Letters*, 2019, 245: 106-109.
[17] X Wang, Z Zhang, Z Hu, et al. Effect of Ni foil thickness on the microstructure of fusion zone during PHS laser welding. *Optics and Laser Technology*, 2020, 125:106014.
[18] K Rubben, H Mohrbacher, E Leirman. Advantages of using an oscillating laser beam for the production of tailed blanks. *SPIE*, 1997, 3097: 228-241.
[19] K Hao, G Li, M Gao, et al. Weld formation mechanism of fiber laser oscillating welding of austenitic stainless steel. *Journal of Materials Processing Technology*, 2015, 225: 77-83.
[20] H Chen, L Deng, J Duan. Picosecond laser welding of glasses with a large gap by a rapid oscillating scan. *Optics Letters*, 2019, 44(10): 2570-2573.
[21] A Mahrle, E Beyer. Modeling and simulation of the energy deposition in laser beam welding with oscillatory beam deflection. *International Congress on Applications of Lasers and Electro-Optics*. 2007, 1805.
[22] G Jiang, C Xi, B Ky, et al. Improving fusion zone microstructure inhomogeneity in dissimilar-metal welding by laser welding with oscillation. *Materials Letters*, 2020, 261: 126995.
[23] Z Jiang, X Chen. H Li, et al. Grain refinement and laser energy distribution during laser oscillating welding of Invar alloy. *Materials & Design*, 2020, 186: 108195.
[24] L Zhao, X Zhang, W Chen, et al. Repression of porosity with beam weaving laser welding. *Transactions of the China Welding Institution*, 2004, 29-32+2.
[25] B Gerhards, O Engels, O OlschoN, et al. Laser beam welding of press hardened ultra-high strength 22MnB5 steel. *Lasers in Manufacturing Conference*, Munich, Germany, 2015, 247.
[26] H Wang, M Nakanishi, Y Kawahito. Dynamic balance of heat and mass in high power density laser welding. *Optical Express*, 2018, 26: 6392–6399 .
[27] L Wang, M Gao, C Zhang, et al. Effect of beam oscillating pattern on weld characterization of laser welding of AA6061-T6 aluminum alloy. *Materials and Design*, 2016, 108: 707-717.
[28] C Wu, H Zhang, J Chen. Numerical simulation of keyhole behaviors and fluid dynamics in laser-gas metal arc hybrid welding of ferrite stainless steel plates. *Journal of Materials Processing Technology*, 2017, 25: 235–245 .
[29] X Chen, X Wang, Q Sun, et al. Improving the mechanical properties of PHS laser welded joints by adding Ni foil to suppress δ-ferrite. *Journal of Materials Research and Technology*, 2020, 9: 5184-5193.